Investigation of continuous casting slag films sampled on site and comparison with laboratory results

Irmtraud Marschall[1)], Nathalie Kölbl[1)], Harald Harmuth[1)] and Guangmin Xia[2)]*

1) Chair of Ceramics, Montanuniversitaet Leoben, Leoben 8700, Austria

2) voestalpine Stahl GmbH, Linz 4020, Austria

Abstract: Slag film samples together with their associated mold fluxes were collected after service during tail out at the voestalpine Stahl GmbH continuous casting machine. The slag films were obtained after casting steel grades different in Al or Ti content and mineralogically investigated. Three distinctive layers could be determined within the slag films. A so called glassy layer, a crystalline layer and a layer, which has been liquid during casting and solidified afterwars, could be observed. Cuspidine ($Ca_4Si_2O_7F_2$) is the prevailing crystal phase in the crystalline layer. Casting alloyed steel grades the structure of the crystalline layer will be modified. With increasing Al_2O_3 content of the slag, due to interactions with the steel, nepheline ($(Na,K)AlSiO_4$) was formed besides cuspidine. Here the distinctive needle like shaped cuspidine is remarkable. With casting steel grades with even more elevated Al content, the slag composition shows a strong decrease of silica and an increase of alumina. Therefore no longer cuspidine but fluorite (CaF_2) and a so far unknown phase rich in alumina are the main crystal phases. When casting steel grades with increased Ti content, perovskite ($CaTiO_3$) will be formed additionally to cuspidine in the crystalline layer.

In addition quench tests of the original mold powders as well as DTA and viscosity measurements of the original mold powder and the slag films were performed. The methods revealed the impact of the Al_2O_3 and TiO_2 pick-up on the crystallization temperature, the phase composition and the viscosity.

Key words: Mold flux, Slag film, Cuspidine, Crystallization, Devitrification

1. Introduction

In the continuous casting process of steel mold fluxes are fed onto the top of the liquid steel in the mold. Liquid slag infiltrates into the channel between the newly formed steel shell and the copper mold and solidifies against the mold wall forming a slag film. This slag film provides both lubrication and heat transfer. Previous investigations [1,9,10] revealed that the slag film shows three distinct layers: a glassy layer in contact with the mold, followed by a crystalline layer formed during casting and a liquid slag layer at the strand side. If the residence time in the gap is longer than approximately 20 min, only a crystalline layer will be found on the mold side [11,12]. It is either formed by crystallization or devitrification. Due to the fact that the heat flux is influenced by the crystalline volume fraction, crystal layer thickness as well as crystal shape and size [1-8], the crystallization behavior of the slag is a matter of particular interest. Crystallization in the slag film depends on the chemical composition, the cooling rate, the temperature and the residence time, which can be several hours [13-15]. Voids and/or pores should be found due to the shrinkage during crystallization or gas formation [2,10,11,13]. It has been observed [2,10] that the chemical composition varies also from the strand to the mold side. Due to its high melting point cuspidine is the dominant

mineral phase in the crystalline layer of fluorine-containing mold slags but within the layer in contact with the mold other mineral phases besides cuspidine were observed [2,4,9,15].

Considering the interactions of slag and steel alumina pick-up by mold slag takes place during the casting process [16-20]. Additionally to the alumina pick-up the alumina content of the slag is increased by the reduction of silica. The latter one is explainable by the low oxygen partial pressure caused by aluminum in the steel which brings about reduction of SiO_2. Due to the modified chemical composition the properties of the mold slag are changed.

In the past numerous laboratory trials were carried out on the investigation of crystallization and devitrification of mold slag [3, 11,14,18, 21-26]. Moreover a computational model has been applied [27]. But so far no investigation concerning the slag film morphology after alumina pick-up has been reported

2. Experimental

2.1 Sample preparation

The investigation was carried out on commercial mold fluxes used at voestalpine Stahl Linz GmbH slab caster. In total 12 slag film samples (SF1-SF12) of three different mold fluxes (MF1-MF3) were collected during tail out after casting 10 different steel grades. The samples were carefully peeled off the mold by a steel hook and cooled down to room temperature on a steel plate. Thereby only the first 10-20 cm of the slag film below the meniscus could be extracted.

The amount of the main elements of the mold fluxes and the slag films are documented in Table 1. Remarkable is the dependency of the slag films Al_2O_3 content on the steel quality. It can be seen that the chemical compositions of the samples MF1-SF1 and MF1-SF2 as well as MF1-SF3 and MF1-SF4 which were in contact with the same steel grade are very similar.

Table 1 Chemical composition of mold fluxes and slag films

Sample	Mold Flux; Chemical composition (weight %)							Sample	steel	Slag film; Chemical composition (weight %)						
	SiO_2	Al_2O_3	$Na_2O+K_2O+Li_2O$	F	MnO	TiO_2	CaO/SiO_2		Al	SiO_2	Al_2O_3	$Na_2O+K_2O+Li_2O$	F	MnO	TiO_2	CaO/SiO_2
MF1	40.1	2.1	7.0	5.7	0.0	0.1	0.93	MF1-SF1	0.11	38.4	3.7	8.5	6.0	0.9	0.0	0.94
								MF1-SF2	0.11	38.3	3.8	7.3	6.1	0.8	0.1	0.96
								MF1-SF3	0.49	31.0	10.88	7.1	7.6	0.3	0.1	1.13
								MF1-SF4	0.48	32.7	10.3	7.4	6.5	0.3	0.0	1.09
								MF1-SF5	0.56	29.8	13.7	7.6	6.7	0.2	0.1	1.22
MF2	37.0	3.8	12.9	10	6.5	0.0	0.55	MF2-SF6	0.77	23.6	28.5	11.7	10.4	1.13	0.0	0.96
								MF2-SF7	0.99	19.3	33.7	11.4	10.8	1.04	0.0	1.16
								MF2-SF8	1.27	15.4	37.9	11.9	10.8	0.5	0.0	1.44
MF3	34.7	3.3	9.9	8.9	0.0	0.0	1.15	MF3-SF9	0.03	33.8	4.4	9.7	9.6	1.8	0.1	1.12
								MF3-SF10	0.04	34.0	6.1	8.8	8.5	1.3	0.3	1.13
								MF3SF11	0.04	33.4	7.9	9.0	8.6	1.3	0.0	1.14
								Mf3-SF12	0.05	31.4	5.3	9.5	9.8	3.0	5.1	1.08

To investigate the devitrification of the original slag of MF1 without steel contact, the mold flux was decarburized at 973K for 7 h in a muffle type furnace. Afterwards it was liquefied in a platinum crucible at 1573K for 5 min. Then this melt was cast into a preheated steel crucible and held at 1173K for 10 min (MF1-OS10), 30 min (MF1-OS30) and 60

min (MF1-OS60), respectively, to investigate the crystalline volume fraction depending on time. After the dwell time the samples were quenched to room temperature. Similar tests were performed with MF2 and MF3 with only 60 min dwell (MF2-OS60 and MF3-OS60). In a second trial the liquid slag of MF1 after heat treatment at 1573K was quenched to room temperature by pouring it into water (MF1-OS240). Thereby, due to the thermal shock the glassy slag burst into fragments. Afterwards this material was annealed for 240 min at 1173K in a steel crucible and quenched to room temperature by plunging the crucible into water.

2.2 Measurement

First the slag films were characterized macroscopically. Based on this specimens for mineralogical investigations were selected. Then X-ray diffraction (XRD), reflected light microscopy and scanning electron microscopy including energy-dispersive X-ray spectroscopy (SEM-EDX) were performed both on the laboratory slag and the slag films. For the determination of the crystallization temperature a simultaneous thermal analysis (STA) was carried out. There ground samples were heated to 1573K using a heating rate of $20Kmin^{-1}$, held for 15 min and cooled down to room temperature with $20Kmin^{-1}$. In addition a dynamic viscosity measurement with a rotary viscometer in oxidizing atmosphere was carried out to investigate the effect of the modified slag composition during casting on the viscosity and break temperature. The samples were heated to 1673K as fast as possible within the crucible and were cooled down with 10 $Kmin^{-1}$ during the measurement. Unfortunately the slag MF2-SF6 crept over the crucible and damaged the equipment. As a consequence further tests with MF2 samples were canceled. Therefore viscosity results are only available for samples of MF1 and MF3.

3. Results

3.1 Macroscopical investigations of the samples taken after service

The slag film samples gained from MF1 and MF3 were even and brittle. Contrary slag films of MF2 were semiliquid when placing on the steel plate and therefore crumpled during sampling. Because of the sampling during tale out, which caused a coating of the slag films by the top slag, the original surfaces on the strand side of all slag films but partly MF2-SF8 cannot be estimated. Only in this case slab imprints observed indicates a slag film thickness of 0.5mm during service. At regions where MF2-SF8 was coated during tail out the maximum slag film thickness was up to 2.5mm. Considering the surface in contact with the mold, fine ripples and fractures are present which are in accordance with former studies [9,13]. Contrary to other observations [10,13] white areas, caused by villiaumite (NaF) segregation could only be observed with MF2-SF7 and MF2-SF8.

3.2 Mineralogical investigation

3.2.1 Crystallization of the original slags

The microscopic investigations of the quench tests of all three mold fluxes reveal that cuspidine ($Ca_4Si_2O_7F_2$) is the dominant phase in all investigated mold fluxes. In general the dendritic crystal growth started at the surface of the slag. In sample MF1-OS60 fluorite has crystallized between the cuspidine dendrites out of the glassy phase as well (Fig.1b).

MF2-OS60 is mainly glassy and shows only some idiomorphic cuspidine crystals and fluorite dendrites (Fig. 1c). Due to its high CaO/SiO_2 ratio MF3-OS60 has got the highest cuspidine amount and hauyn $(Na,Ca)_{8\text{-}4}[(SO_4)_{2\text{-}1}(AlSiO_4)_6]$ as second phase (Fig. 1d). As could be expected the specimen with 10 min dwell time (MF1-OS10) shows the highest amount of glassy phase (Table 2). With increasing dwell time the volume fraction of cuspidine and fluorite increases, whereas the crystal size of cuspidine remains almost unaffected. It seems that except for fluorite the crystallization comes to an end after 30 min (MF1-OS30). Even after 60 min dwell time (MF1-OS60) crystallization did not approach the specimen center.

The microstructure of MF1 after reheating (MF1-OS240) is different from the crystallized sample. In Fig.1a the fragments of the glassy slags are still visible. During devitrification small cuspidine needles and fluorite were formed within those pieces. At the boundaries of these fragments relatively large fluorite crystals and in contrast to MF 1-OS 10-60 diopside was formed. The amount of the glassy phase of MF1-OS240 is higher compared to MF1- OS30 and MF1-OS60 (Table 2).

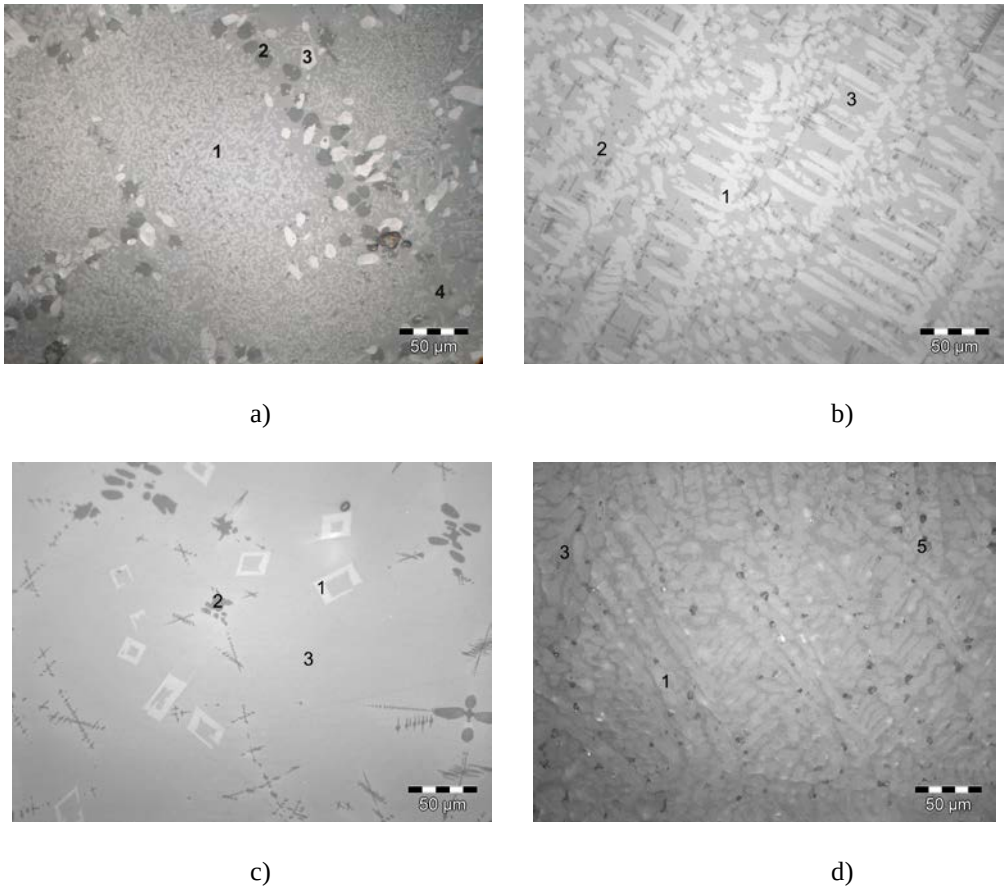

Fig. 1 a) Reflected light micrograph of the original slag reheated at 1173K for 4h after quenching from 1573K to room temperature (MF1-OS 240). b-d): Reflected light micrograph of the original slag annealed for 60min at 1173K after quenching from 1573K b) MF1-OS60, c) MF2-S60 and d) MF3-S60. 1: cuspidine, 2: fluorite, 3: glassy phase, 4: diopside, 5: hauyne

Table 2 Phase compositions of the original slags after annealing at 900°C determined by Rietveld refinement

Sample		MF1-OS240	MF1-OS10	MF1-SO30	MF1-OS60	MF2-OS60	MF3-OS60
Quenched to °C		20 Reheated to 900	900	900	900	900	900
Dwell time	min	240	10	30	60	60	60
Glassy phase	mass%	52	87	39	39	49	5
Cuspidine	mass%	34	12	54	53	44	95
Fluorite	mass%	5	1	7	8	7	
Diopside	mass%	9					

3.2.2 Slag films taken from service

Slag films gained from MF1

The microscopic investigations showed that all five slag films have formed three different layers: A basically glassy layer (L1) with a small amount of crystal phase in contact with the mold, a well crystallized layer (L2) and a glassy layer (L3) which is supposed to be increased during tail out due to coating. In some cases the crystallized layer is split into two sub layers (L2.1 and L2.2). A more detailed investigation of the samples reveals a distinctive microstructure of the slag films of each steel grade.

As may be seen from Fig. 2 the slag films MF1-SF1 and MF1-SF2 in contact with steel grade 1 are clearly distinguishable into the three sub layers. Noticeable is the crystalline layer L2, which consists of cuspidine crystals with a maximum elongation of approximately 100 µm in a glassy matrix. The border to the former liquid slag is well defined. Table 3 shows a comparison of all layers. From this a considerable decrease of the CaO/SiO_2 ratio and an increase of Al_2O_3 and Na_2O for L1 in contact with the mold compared to the other layers can be seen. Due to this modified composition and the low temperatures mainly small sized cuspidine (<1µm), needle shaped fluorrichterite ($(Ca_2(Mg,Fe,Al)_5(Al,Si)_8O_{22}F_2)$) and fluorite are formed. At the interface of L1 and L2 also diopside is detected.

In contrary to MF1-SF1 and MF1-SF2 the crystalline layer of MF1-SF3 and MF1-SF4 can be divided into two sub layers: L2.1 and L2.2 (see Fig. 3). Within L2.2 the Cao/SiO_2 ratio is increased from 0.97 to 1.1 whereas it is decreased to 0.8 within L2.1. From the mineralogical point of view the sub layer L2.2 is comparable to L2 of MF1-SF1 and MF1-SF2 showing cuspidine as the only mineral phase but the crystal shape within SF3 and SF4 is different. Due to the higher Al_2O_3 content of MF1-SF3 and MF1-SF4 nepheline ($(Na,K)AlSiO_4$) was xenomorphically formed in L2.1 besides cuspidine and because of the crystallization of nepheline the highest Al_2O_3 content of SF3 and SF4 can be found within this layer. In contact with the mold the structure of L1 is not totally glassy. Cuspidine is dominating in a glassy matrix. Nepheline is the second crystalline phase within L1. Characteristic for this layer are large spherical pores.

A considerable modification compared to the original slag exhibits MF1-SF5 (see Table 3). Even though the microstructure of the crystalline layers differs in dependence on the vertical position within these samples, again two sub layers can be distinguished. From Fig. 4 it can be seen that L2.1 consists of needle shaped cuspidine crystals with a maximum elongation of approximately 50 µm. Between these needles nepheline and pyroxene are present. In L2.2 the cuspidine crystal size is increased in comparison to L2.1 and in some regions nepheline and pyroxene can be found as well. If cuspidine is the only crystal phase the boundary to L3 is sharp, otherwise often it appears diffuse. In this case

also L1 is not uniform. Within 40 µm the structure changes from glassy to crystalline showing fine crystals of cuspidine.

Summing up, this investigation reveals that in case of an extensive Al_2O_3 pick-up not only cuspidine is the dominant solid phase in the well crystallized layer but also nepheline can be formed. If cuspidine is the only crystalline phase, the highest CaO/SiO_2 ratio can be found in this area of the slag film. If nepheline is formed too, the CaO/SiO_2 ratio is lowest compared to the other slag film layers.

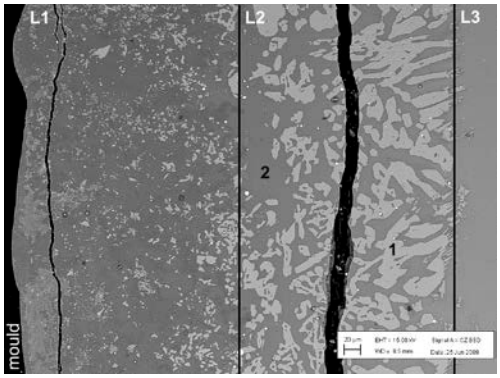

Fig. 2 Back scattered electron image of slag film MF1-SF1 1. 1: cuspidine, 2: glassy phase

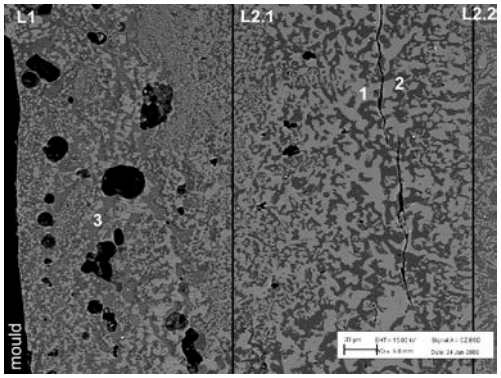

Fig. 3 Back scattered electron image of slag film MF1-SF4 2. 1: cuspidine, 2: nepheline, 3 glassy phase

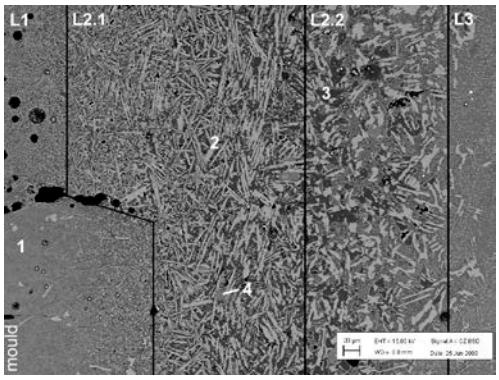

Fig. 4 Back scattered electron image of slag film MF1-SF5. 1: glassy phase, 2: cuspidine, 3: nepheline, 4: pyroxene

Table 3 Summary of the slag film layers for MF1-SF1 to MF1-SF5

	Chemical distribution				Mineral phase				
Sample	layer	CaO/SiO_2	Al_2O_3/ $Al_2O_{3,os}$	Na_2O/ Na_2O_{os}	Cuspidine ($Ca4SiO_2$)	Fluorite (CaF_2)	Fluorrichterite ($Ca_2(Mg,Fe,Al)_5(Al,Si)_8O_{22}F_2$)	Nepheline ($(Na,K)AlSiO_4$)	Pyroxene
MF1-SF1 and MF1-SF2	L1	0.3	3.6	1.7	x	x	x		
	L2	0.9	1.6	0.9	x				
	L3	0.8	1.6	1.0					
MF1-SF3 and MF1-SF4	L1	0.9	6.4	1.4	X			X	
	L2.1	0.8	7.4	1.4	X			X	
	L2.2	1.1	5.2	1.0	x				
	L3	0.9	5.1	1.1					
MF1-SF5	L1	1.1	7.1	0.9	X				
	L2.1	1.0	8.5	1.2	X			X	X
	L2.2	1.1	7.6	1.1	x			X	x
	L3	1.1	8.2	1.2					

Slag films of MF2

Contrary to the MF1 slag films, slag films of MF2 exhibit no classical slag layer formation. Crystallization takes place in contact with the mold, where according to previous investigations a glassy layer should be present. Due to the high Al_2O_3 and the low SiO_2 content fluorite was formed within spherical pores in the former liquid slag on the strand side (Fig. 5). In Table 4 an overview of the chemical distribution within the slag film samples is given. L2 indicates the crystalline parts of the slag films and L3 the former liquid slag.

Coming into detail, in MF2-SF6 a small layer (L2.1) can be observed which has four times the fluorine content of the original mold flux composition. As can be seen from Fig. 6 it is mainly composed of fluorite. LiF was formed within a sodium alumina silicate phase (NAS) ($Na_{0,775}$ $Al_{0,775}$ $Si_{0,225}$ O_2) according to [28]. Adjacent is a layer consisting of a sodium alumina silicate phase which merges into a layer consisting of liquid slag and fluorite. In this layer (L2.2) the Al_2O_3 content is 7.8 times the content of the original mold flux.

MF2-SF7 is the least crystalline sample. Only a small crystalline layer (L2) consisting of fluorite and sodium alumina silicate phase can be observed attached to the mold (Fig. 7).

The slag film structure of MF2-SF8 is different from the previous described slag films (Fig. 8). This one was in contact with the steel with the highest Al content. Therefore MF2-SF8 has the highest Al_2O_3 content of all investigated samples. Due to the reduction of the slag film´s SiO_2 content the CaO/SiO_2 ratio increased to 1.44 in total. As a consequence the crystallization tendency increased drastically. A XRD analysis (Fig. 9) revealed, that the slag film is mainly crystalline. No hump indicating a glassy phase is visible in the XRD spectrum. Instead besides fluorite, villiaumite, cuspidine and oldhamite (CaS) residual peaks could be detectedt which did not match with any mineral phase included in the ICDD PDF4+ database [29]. This phase shows a maximum peak at 2 Θ 30.122. The other main peaks are at 2 theat 25,639, 31,468, 15,605 and 23,998. Its mean chemical composition is given as follows: 7.8 mol% F, 10.5 mol% Na, 17.1 mol% Al, 5.3 mol% Si, 6.7mol% Ca and 40 mol% O. Considering the slag film structure, in contact with the mold an up to 47 µm thick layer (L2.1) of villiaumite has been formed. Adjacent is a layer (L2.2) which has a remarkable high CaO/SiO_2 ratio of 9.3 and a SO_3 content of 3wt% but no Al_2O_3. It consist mainly of fluorite. Oldhamite ((Ca,Mg, Fe)S) and neighborite ($NaMgF_3$) can be encountered in-between. This layer is followed by a dens fluorite layer (L2.3) including some cuspidine crystals. The thicknesss of L2.2 and L2.3 is in total up to 200µm.; but the main slag film is made of the needlelike shaped phase rich in alumina described above which can be observed in layer L2.4 and L2.5.

Summing up, due to the drastic increase of Al_2O_3 cuspidine is no longer the dominating crystal phase of the slag film structure. Instead Fluorite and a phase rich in alumina are formed.

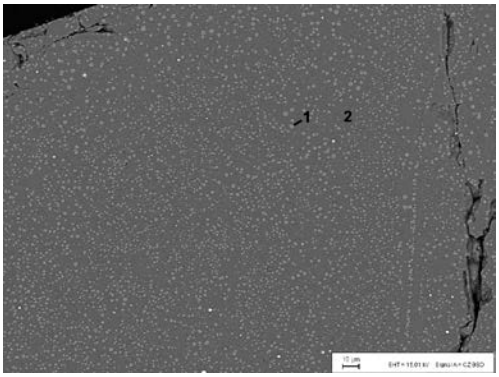

Fig. 5 Back scattered electron image of slag MF2-SF8. 1: fluorite, 2: glassy phase

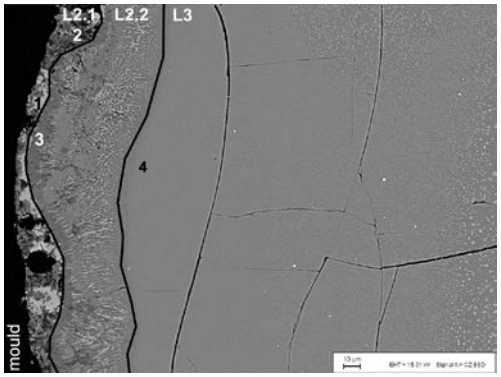

Fig. 6 Back scattered electron image of slag film MF2-SF6. 1: fluorite, 2: LiF, 3: $Na_{0,775}$ $Al_{0,775}$ $Si_{0,225}$ O_2, 4: glassy phase

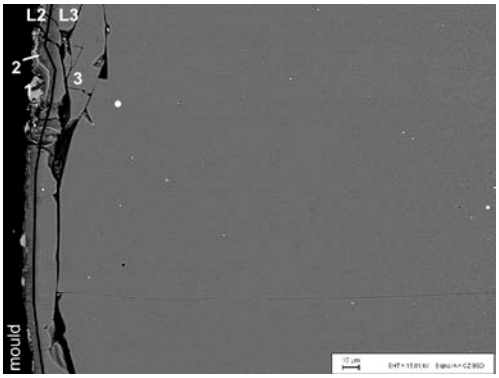

Fig. 7 Back scattered electron image of slag film MF2-SF6. 1: fluorite, 2: $Na_{0,77}$ $Al_{0,775}$ $Si_{0,225}O_2$, 3: glassy phase

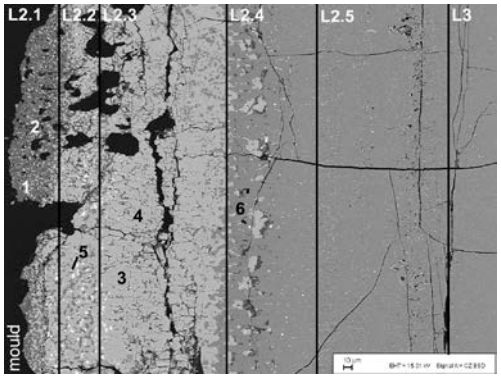

Fig. 8 Back scattered electron image of slag film MF2-SF8. 1: fluorite, 2: villiaumite, 3: fluorite, 4: neihgborite, 5: oldhamite, 6:phase rich in alumina

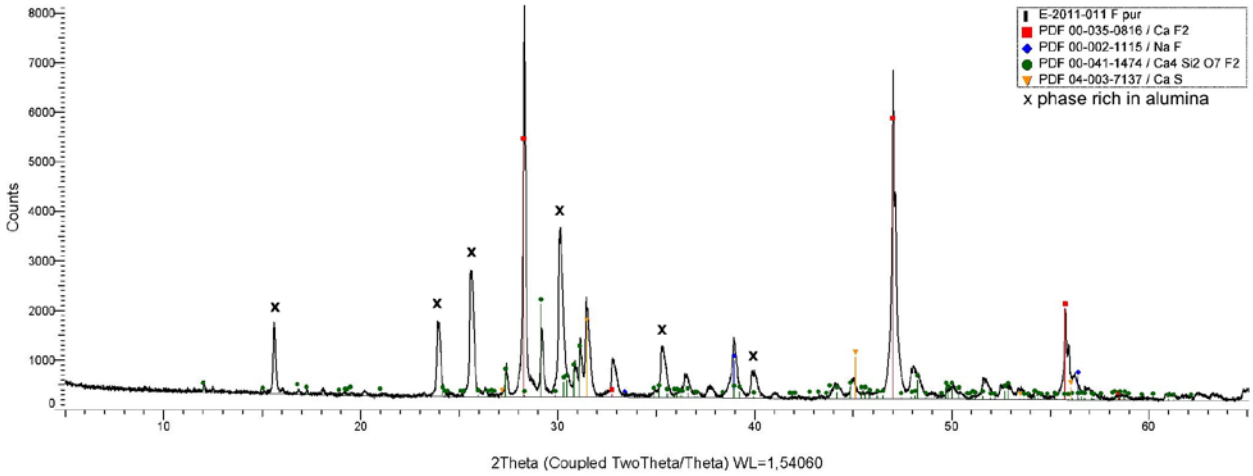

Fig. 9 XRD spectrum of MF2-SF8.

Table 4 Summary of the slag film layers of MF2-SF6 to MF2-SF8

	Chemical distribution					Mineral phases							
Sample	layer	C/S	Al_2O_3/ $Al_2O_{3,os}$	Na_2O/ $Na_2O_{,os}$	F/F_{os}	Fluorite (CaF_2)	LiF	NAS ($Na_{0,77}$, $Al_{0,775}$, $Si_{0,225,}O_2$)	Villiaumite (NaF)	Neighborite ($NaMgF_3$)	Oldhamite (CaS)	Cuspidine ($Ca_4Si_2O_7F_2$)	Phase rich in alumina
MF2-SF6	L2.1	0.7	2.9	1.9	4.0	x	x	x					
	L2.2	0.7	7.8	1.9	1.2	x		x					
	L3	1.0	8.2	1.0	1.0	x							
MF2-SF7	L2	1.1	9.0	1.2	1.2	x		x					
	L3	0.9	9.3	1.0	1.1	x							
MF2-SF8	L2.1	8.4	0	3.4	4.1	x			x	x			
	L2.2	9.3	0	0.3	3.4	x				x	x		
	L2.3	3.7	1.0	0.2	2.9	x						x	
	L2.4	1.7	10.2	1.4	1.1	x							x
	L2.5	1.5	10.2	1.1	1.0	x							x
	L3	1.6	7.0	1.2	1.2	x							

Slag films of MF3

Due to MF 3´s CaO/SiO_2 ratio of 1.15 its associated slag films are mainly crystalline. The cooling rate during sampling was too low to prevent the liquid slag film layer from crystallization. All slag films have in common, that their total dimension as well as their crystalline layer increase with increasing depth in the mold. 20 cm below the meniscus level the crystalline layer is more than the double of the size than that one 5 cm below the meniscus level. The examples given in Fig. 10-13 and Table 5 are located 20-25cm below the meniscus.

With sample MF3-SF1 the border between the crystalline layer and the former liquid layer can only be estimated. The Al_2O_3 content is highest in the layer attached to the mold. As can be seen from Fig. 10 this layer is not glassy but contains also small sized cuspidine. Between the cuspidine crystals jadeite ($NaAlSi_2O_6$) and villiaumite occur. Within the crystalline layer the cuspidine crystal size is enhanced, but still very small compared to MF3-SF10 and MF3-SF11. The boundary to the crystalline layer is not parallel to the mold.

Different from MF3-SF1 is the microstructure of MF3-SF10 (Fig.11). The dense crystalline layer (L2) consists of up to 300µm long cuspidine crystals which are orientated parallel to the temperature gradient. The CaO/SiO_2 ratio is 1.5 and as can be seen from Table 5 the Al_2O_3 and Na_2O content are drastically decreased. Fig. 11 shows that a rupture within the crystalline layer occurs. As a consequence the glassy layer attached to the mold is not uniform. The area next to the fracture (L1.1) exhibits a CaO/SiO_2 ratio of 0.7 and the highest Al_2O_3 and Na_2O contents compared to the other layers. Due to the change in chemical composition jadeite is the dominating phase within this area. Whereas the main part of the glassy layer (L1.2) consist mainly of small sized cuspidine crystals in a glassy matrix. The slag film structure of MF3-SF11 (Fig.12) is similar to the structure of MF3-SF10. Likewise the crystalline layer consists of large cuspidine crystals and as well this dense layer is interrupted by a glassy layer enriched in Al_2O_3 and Na_2O.

The biggest difference of the slag film structure exhibits MF3-SF12. In this case a steel grade containing considerable amounts of Ti was casted. As a consequence the TiO_2 content of the slag film increased to 5.1wt%. Remarkable is the slag film structure which was found to be glassy even 17cm below the meniscus level. 20 cm below the meniscus level this slag film was crystalline, too (Fig. 13). Small perovskite ($CaTiO_3$) crystals were formed between cuspidine

dendrites. A glassy and crystalline layer is not exactly distinguishable. Even the chemical composition is constant from the strand to the mold side (Tab.5).

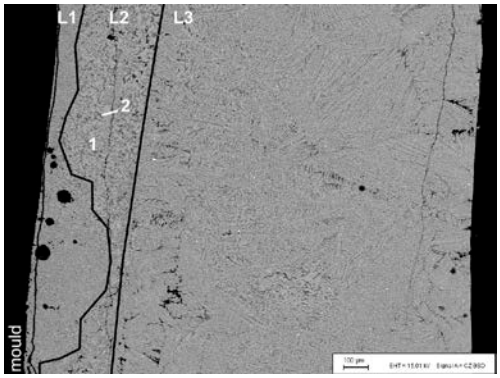

Fig. 10 Back scattered electron image of slag MF3-SF9. 1: cuspidine, 2: jadeite

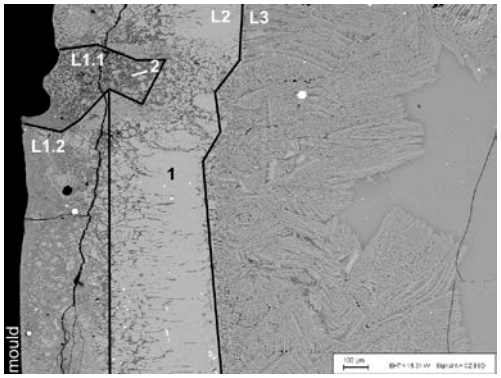

Fig. 11 Back scattered electron image of slag MF3-SF10. 1: cuspidine, 2: jadeite

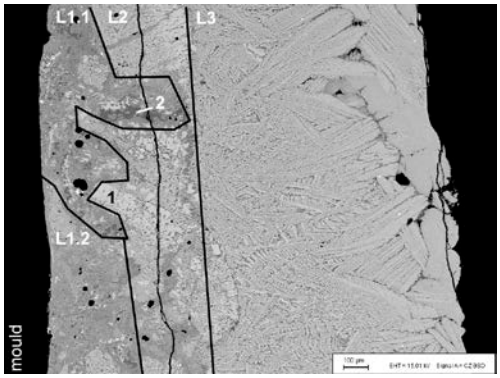

Fig. 12 Back scattered electron image of slag MF3-SF11. 1: cuspidine, 2: jadeite

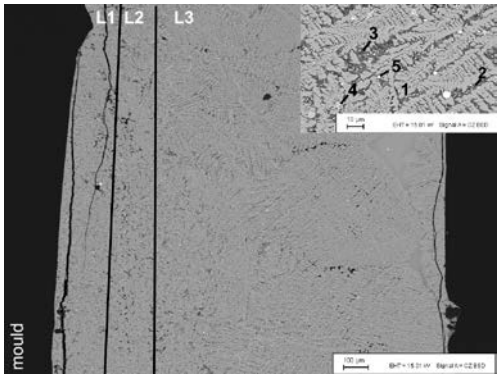

Fig. 13 Back scattered electron image of slag MF3-SF12 1: cuspidine, 2: jadeite, 3: villiaumite, 4:perovskite; 5. oldhamite

Table 5 Summary of the slag film layers for MF3-SF9 to MF3-SF12

	Chemical distribution				Mineral phases			
Sample	layer	C/S	Al_2O_3/ $Al_2O_{3,os}$	Na_2O/ $Na_2O_{,OS}$	Cuspidine ($Ca_4Si_2O_7F_2$)	Jadeite ($NaSiAl_2O_6$)	Villiaumite (NaF)	Perovskite ($CaTiO_3$)
MF3-SF9	L1	1.1	1.1	1.1	x	x	x	
	L2	1.5	1.4	1.0	x	x		
	L3	1.1	1.0	1.0				
MF3-SF10	L1.1	0.7	3.2	1.5	x	x	x	
	L1.2	1.2	2.2	0.7	x		x	
	L2	1.5	0.6	0.3	x			
	L3	1.1	1.6	1.0				
MF3-SF11	L1.1	0.8	4.8	1.1	x	x		
	L1.2	1.0	3.5	0.9	x	x	x	
	L2	1.1	2.3	0.9	x			
	L3	1.1	1.8	1.0				
MF3-SF12	L1	1.1	1.7	1.0	x	x	x	x
	L2	1.1	1.6	1.0	x	x	x	x
	L3	1.1	1.6	1.0				

3.3 Simultaneous thermal analysis (STA)

Additionally to the microscopical investigations a STA was carried out. The results are listed in Table 6. For MF1 the crystallization temperature of the slag film MF1-SF2 is decreased according to the original mold flux, but with increasing Al_2O_3 content the crystallization temperature increases compared to the original mold slag MF1-OS. Contrary no peak could be observe when measuring the crystallization temperature of MF2-OS, but with increasing Al_2O_3 content the crystallization temperature increases as well. Remarkable is the high crystallization temperature of 1328K for MF2-SF9. With MF3 the crystallization temperature is increased by the addition of Al_2O_3, but the presencs of TiO_2 causes a decrease of the crystallization temperature of MF3-SF12 compared to the other slag film samples.

Table 6 Crystallization temperature obtained by STA

Sample		Crystallization temperatur in K	Sample		Crystallization temperatur in K	Sample		Crystallization temperatur in K
MF1	MF1-OS	1302	MF2	MF2-OS	no crystallization	MF3	MF3-OS	1274
	MF1-SF2	1148		MF2-SF6	1122		MF3-SF9	1439
	MF1-SF3	1178		MF2-SF7	1152		MF3-SF10	1442
	MF1_SF5	1325		MF2-SF8	1328		MF3-SF11	1426
							MF3-SF12	1389

3.4 Viscosity

As shown in Fig. 14 the viscosity of MF 1 is increased with increasing Al_2O_3 content of the slag films. The Break Temperature of the slag films is in all cases higher than the break temperature of the original slag. In the case of MF1-SF5 the difference is 85K. With MF3 the viscosity as well as the break temperature is decreased due to the TiO_2 increase (Fig.15). For MF3-SF12 the break temperature is 197K lower than the break temperature of the original slag MF3-OS.

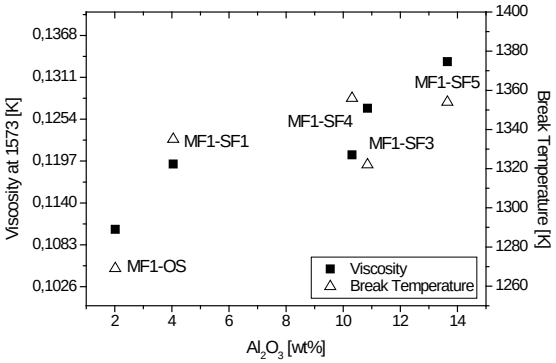

Fig.14 Viscosity at 1573K and Break Temperature of the original slag (MF1-OS) and its corresponding slag films (SF) in dependence on the Al_2O_3 content

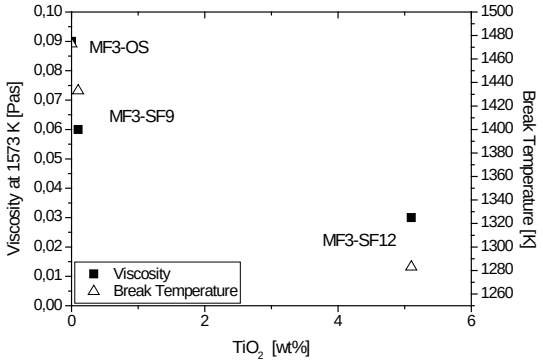

Fig.15 Viscosity at 1573K and Break Temperature of the original slag (MF3-OS) and its corresponding slag films (SF) in dependence on the TiO_2 content

4. Discussion

The investigation emphasizes the influence of the steel composition on the slag film properties. The addition of Al_2O_3 leads to an increasing crystallization temperature for all samples. When TiO_2 is added the crystallization temperature decreases. The viscosity is increased by additional Al_2O_3 as well. Unfortunately the samples of MF2 were not possible to measure. But from the experiences during sampling it was estimated that the viscosities of these samples

are much higher compared to the others due to their high Al_2O_3 content. Therefore it can be concluded that Al_2O_3 acts as a network former for all specimens investigated. TiO_2 on the other hand causes a decrease of the viscosity.

The mineralogical investigations of the original mold slag show once again the impact of the CaO/SiO_2 ratio on the crystallization behavior. Considering the results of MF1 original slag after increasing dwell time and of the slag films after service both the crystallization of the liquid phase and the devitrification of a glassy phase take place during service. Whereas the formation of the crystalline layer is caused by crystallization, the formation of the crystals in contact with the mold is dominated by devitrification. With SiO_2 based mold powders in general the Al_2O_3 content and the Na_2O content is highest in the layer attached to the mold. As a consequence sodium-aluminium-silicates are likely to be formed in this area. The crystalline layer is mainly composed of cuspidine. Therefore the CaO/SiO_2 ratio is highest within the crystalline layer.

In the case of minor modification of the chemical composition during service the mineralogical compositions of the original slag and the slag films are comparable. With increasing differences in the Al_2O_3 content the crystallization behavior of the slag films deviates from the original slag. The phase composition as well as the crystal shape is strongly affected by the alteration of the chemical composition. If the slag film composition changes from silica based to alumina based fluorite will be formed instead of cuspidine. Remarkable was the structure of MF-SF8. Here the CaO/SiO_2 ratio was increased from 0.55 to 1.55 compared to the mold flux and the Al_2O_3 content increased from 3.8 to 37.9. As a consequence in contrary to the original slag MF2-OS60 and the other slag films gained from this mold flux most of the slag film structure was crystalline, consisting of fluorite at the mold side and a so far not identified phase rich in alumina composition. Its mean chemical composition is given as follows: 7.8 mol% F, 10.5 mol% Na, 17.1 mol% Al, 5.3 mol% Si, 6.7mol% Ca and 40 mol% O.

The results were correlated with the logged integral heat flux, but because of deviating casting parameters so far no assured results could be gained.

5. Conclusions

The crystallization behavior of three commercial mold fluxes and in total twelve corresponding slag films was investigated. In total 10 steel grades were cast with significant difference in the Al or Ti content.

Key results are summarized below:

- Due to aluminum pick-up the Al_2O_3 content as well as the CaO/SiO_2 ratio of the slag films was modified.
- As a consequence the viscosity and the crystallization temperature increased with increasing Al_2O_3 content.
- The microstructures of the slag films were strongly affected by Al_2O_3 pick-up.
- In case of an alteration of the chemical composition from silica based to alumina based, fluorite and a phase rich in alumina are the dominating crystal phases.
- In case of a TiO_2 increase, the viscosity and the crystallization temperature will be decreased and perovskite will be formed as an additional mineral phase.

Acknowledgement

The research program of the competence center “Advanced Metallurgical and Environmental Process Development” (K1-MET) is supported within the Austrian program for competence centers COMET (Competence Center for Excellent Technologies) with funds of the Federal Ministry for Transport, Innovation and Technology, the Federal Ministry of Economy, the province of Upper Austria and Styria, the Styrian Business Promotion Agency, of the Tyrol and the Tyrolian Future Foundation.

References

[1] M. Susa, K. C. Mills, M. J. Richardson, R. Taylor, D. Stewart. Thermal properties of slag films taken from continuous casting mold. *Ironmaking Steelmaking*, 1994, 21 (4), p279-286

[2] H. Nakada, M. Susa, Y. Seko, M. Hayashi, K. Nagata. Mechanism of heat transfer reduction by crystallization of mold flux for continuous casting. *ISIJ Int*., 2008, 48 (4), p446-453

[3] M. Hayashi, K. Matsuo, K. Nagata and H. Nakada. Effect of crystalline morphology on heat transfer through mould flux. *Proc. VIII Int. Conf. on 'Molten Slags, Fluxes and Salts'*, (Santiago, Chile), 2009, Gecamin Ltd, p1091-1100

[4] K.C. Mills, A.B. Fox, R.P. Thackray and Z. Li. The performance and properties of mould fluxes. *Proc. VII Int. Conf on 'Molten Slags, Fluxes and Salts'*, (Cape Town, South Africa), 2004, South Africa Institute of Mining & Metallurgy, p713-721

[5] M. Emi. The mechanisms for sticking type break-outs and new developments in continuous casting mold fluxes. *Proc. 'Steelmaking Conference'*, Vol. 74, (Warrendale, PA) 1991, ISS, p623-630

[6] J. Choo, H. Shibata, T. Emi and M. Suzuki. Radiative heat transfer through mold flux film during initial solidification in continuous casting of steel. *ISIJ Int*., 1998, 38 (3), p440-446

[7] M. Kawamoto, Y. Tsukaguchi, N. Nishida, T. Kanazawa, S. Hiraki. Improvement of the intitial stage of solidification by using mild cooling mold powder. *ISIJ Int.*, 1997, 37 (2), p134-139

[8] W. Wang, K. Blazek, A. Cramb. The Effect of the Transition Metal Oxide Content of a Mold Flux on the Radiation Heat Transfer Rates Metall. *Mater. Trans. B*, 2008, 39B, p66-74

[9] B. Stewart, N. Jones, K. Bain, M. McDonald, R. Burniston, M. Bugdol, V. Ludlow. Development of the mould slag film and its impact on the surface quality of continuously cast semis. *Proc. VIII Int. Conf. on 'Molten Slags, Fluxes and Salts'*, (Santiago, Chile), 2009, Gecamin Ltd., p1061-1071

[10] B. Stewart, M. McDonald, M. Hopkins, R. Burniston. Understanding the role of mould slag and slag film in surface quality of continuously cast semis. *Proc. 6th ECCC*, (Riccione, Italy), 2008, AIM, CD-ROM

[11] W. Wang, W. Cramb. Study of the Effects of the Mold Surface and Solid Mold Dlux Crystallization on Rediative Heat Transfer Rates in Continuous Casting. *Steel Research int*, 2008, 79 (4), p271-277

[12] C. Mills. Continuous casting powders and their effect on surface quality and sticker breakouts. *Proc. V Int. Conf. on 'Molten Slags, Fluxes and Salts' Molten Slags, fluxes and salts ’*, (Sydney, Australia), 1997, Iron and Steel Society of Aime, p675-682

[13] P. Hooli. Study on the layers in the film originating from the casting powder between steel shell and mould and associated phenomena in continuous casting of stainless. PhD thesis, University of Technology, Helsinki, Finland, 2007

[14] H. Nakada, M. Susa, Y. Seko, M. Hayashi, K. Nagata. Mechanism of heat transfer reduction by crystallization of mold flux for continuous casting. *ISIJ Int*., 2008, 48(4), p446-453

[15] Y. Kashiwaya, C. E. Cicutti, A. W. Cramb. Crystallization behavior of mold slags. *ISIJ Int*., 1998, 38, p357-365

[16] V. Ludlow, B. Harris, S. Riaz, A. Mormanton. Continuous casting mould powder and casting process interaction: why powders do not always work as expected. *Proc. VII Int. Conf on 'Molten Slags, Fluxes and Salts'*, (Cape Town, South Africa), 2004, South Africa Institute of Mining & Metallurgy, p723-729

[17] R.-H. Gronebaum and J. Pischke. Proc. 49. The function of mould fluxes and the estimation of its properties by thermal analysis. *Internationales Feuerfest-Kolloquium*, (Aachen, Germany), 2006, TU Bergakademie Freiberg, p211-214

[18] L. Courtney, S. Nuortie-Perkkiö, C. A. G. Valadares, M. J. Richardson, K. C. Mills. The crystallization of slag films formed in continuous casting . *Proc. VII Int. Conf on 'Molten Slags, Fluxes and Salts'*, (Stockholm – Helsinki), 2000, CD-ROM

[19] T. Nakano, T. Kishi, K. Koyama, T. Komai. S. Naitoh. Mold powder technology for continuous casting of aluminium-killed steel. *Transactions ISIJ* 1984, 34, p950-956

[20] Th. Do, K. W. Lange, Aufnahme von Tonerde durch Stranggießpulver. *Steel Research*, 1986, 57, p444-451

[21] R. Carli, C. Right. Mould flux crystallization: A kinetic study. *Proc. VII Int. Conf on 'Molten Slags, Fluxes and Salts'*, (Cape Town, South Africa), 2004, South Africa Institute of Mining & Metallurgy, p821-826

[22] K. Chatterjee, G. I. Zhmoidin. The phase equilibrium diagram of the system $CaO\text{-}Al_2O_3\text{-}CaF_2$. *J. Mat. Sci*., 1972, 7, p93-97

[23] P. Grieveson, S. Bagha, N. Machingawuta, K. Liddell, K. C. Mills. Physical properties of casting powders. Part 2: Mineralogical constitution of slags formed by powders. *Ironmaking Steelmaking*, 1988,15, p181-186

[24] K. Tsutsumi, T. Nagasaka, M. Hino, Surface roughness of solidified mold flux in continuous casting process. *ISIJ Int*.,1999, 39, p1150-1159

[25] Orrling, Y. Kashiwaya, S. Sridhar, A. W. Cramb. “In situ” observations and thermal analysis of crystallization phenomenon in mold slags. *Proc. VII Int. Conf on 'Molten Slags, Fluxes and Salts'*, (Stockholm – Helsinki), 2000, CD-ROM

[26] H. Mizuno, H. Esaka, K. Shinozuka, M. Tamur. Analysis of the crystallization of mold flux for continous casting of steel. *ISIJ Int.*, 2008, 48 (3), p277-28

[27] Y. Meng. G. Thomas Simulation of microstructure and behavior of interfacial mold slag layers in continuous casting of steel. *ISIJ Int.*, 2006, 46 (5), p660-669

[28] ICDD PDF card 04-010-3960. Reference J.G. Thompson, R.L.Withers, A. Melnitchenko, S.R. Palethorpe. Cristobalite-Related Phases in the NaAlO2-NaAlSiO4 System. I. Two tetragonal and two orthorhombic structures. *acta crystallogr., Sec. B: Struct. Sci.*, 1998, 54, p531-546

[29] ICDD PDF-4 2010 RDB